Mechanical Weyl Modes in Topological Maxwell Lattices

D. Zeb Rocklin, Bryan Gin–ge Chen, Martin Falk, Vincenzo Vitelli, and T. C. Lubensky

Phys. Rev. Lett. **116**, 135503 — Published 1 April 2016

DOI: 10.1103/PhysRevLett.116.135503

Mechanical Weyl Modes in Topological Maxwell Lattices

D. Zeb Rocklin,[1] Bryan Gin–ge Chen,[2,*] Martin Falk,[3] Vincenzo Vitelli,[2] and T. C. Lubensky[4]

[1] *Department of Physics, University of Michigan, 450 Church St. Ann Arbor, MI 48109, USA*
[2] *Instituut-Lorentz, Universiteit Leiden, 2300 RA Leiden, The Netherlands*
[3] *Department of Physics, Massachusetts Institute of Technology, 77 Massachusetts Avenue Cambridge, MA 02139-4307, USA*
[4] *Department of Physics and Astronomy, University of Pennsylvania, Philadelphia, PA 19104, USA*

(Dated: March 3, 2016)

We show that two-dimensional mechanical lattices can generically display topologically protected *bulk* zero-energy phonon modes at isolated points in the Brillouin zone, analogs of massless fermion modes of Weyl semimetals. We focus on deformed square lattices as the simplest Maxwell lattices, characterized by equal numbers of constraints and degrees of freedom, with this property. The Weyl points appear at the origin of the Brillouin zone along directions with vanishing sound speed and move away to the zone edge (or return to the origin) where they annihilate. Our results suggest a design strategy for topological metamaterials with bulk low-frequency acoustic modes and elastic instabilities at a particular, tunable finite wavevector.

PACS numbers: 62.20.D-, 03.65.Vf

Topological properties of the energy operator and associated functions in wavevector (momentum) space can determine important properties of physical systems [1–3]. In quantum condensed matter systems, topological invariants guarantee the existence and robustness of electronic states at free surfaces and domain walls in polyacetylene [4, 5], quantum Hall systems [6, 7] and topological insulators [8–13] whose bulk electronic spectra are fully gapped (i.e. conduction and valence bands separated by a gap at all wavenumbers). More recently topological *phononic* and *photonic* states have been identified in suitably engineered classical materials as well, [14–33] provided that the band structure of the corresponding wave-like excitations has nontrivial topology.

A special class of topological mechanical states occurs in *Maxwell lattices*, periodic structures in which the number of constraints equals the number of degrees of freedom in each unit cell [34]. In these mechanical frames, zero-energy modes and states of self stress (SSS) are the analogs of particles and holes in electronic topological materials [16]. A zero energy (frequency) mode is the linearization of a *mechanism*, a motion of the system in which no elastic components are stretched [19, 20]. States of self stress on the other hand guide the focusing of applied stress and can be exploited to selectively pattern buckling or failure [18]. Such mechanical states can be topologically protected in Maxwell lattices, such as the distorted kagome lattices of Ref. 16, in which no zero modes exist in the *bulk* phonon spectra (except those required by translational invariance at wavevector $\boldsymbol{k} = 0$). These lattices are the analog of a fully gapped electronic material. They are characterized by a topological polarization equal to a lattice vector $\boldsymbol{R}_T$(which can be zero) that, along with a local polarization $\boldsymbol{R}_L$, determines the number of zero modes *localized* at free surfaces, interior domain walls separating different polarizations, and dislocations [17]. Because $\boldsymbol{R}_T$ only changes upon closing the bulk phonon gap, these modes are robust against disorder or imperfections.

In this paper we demonstrate how to create topologically protected zero modes and states of self-stress that extend throughout a sample. These enable the topological design of bulk soft deformation and material failure in a generic class of mechanical structures. As prototypes, we study the distorted square lattices of masses and springs shown in Fig. 1, and we show that they have phases that are two-dimensional mechanical analogs of Weyl semimetals [35–39]. In the latter materials, the valence and conduction bands touch at isolated points in the Brillouin zone (BZ), with the equivalent *phonon* dispersion for the mechanical lattice shown in Fig. 1(a). Points at which two or four bands touch are usually called Weyl and Dirac points, respectively. These points, which are essentially wavenumber vortices in 2D and hedgehogs in 3D, are characterized by a winding or Chern number [1, 3] and are topologically protected in that they can disappear only if points of opposite sign meet and annihilate or if symmetry-changing terms are introduced into the Hamiltonian. Weyl semimetals exhibit lines of surface states at the Fermi level that terminate at the projection of the Weyl points onto the surface BZ. Weyl points have also been predicted [40] and observed [41] in photonic crystals and certain mechanical systems with pinning constraints that gap out translations [23]. In contrast, our examples consist of ordinary spring networks which suggests that the Weyl phenomenon is in fact generic to Maxwell lattices of sufficient complexity.

Our distorted square lattices are defined by the components of their two primitive lattice vectors and their four basis vectors, for a twelve-dimensional full phase space. We restrict our attention to a representative two-dimensional space by varying only the components of

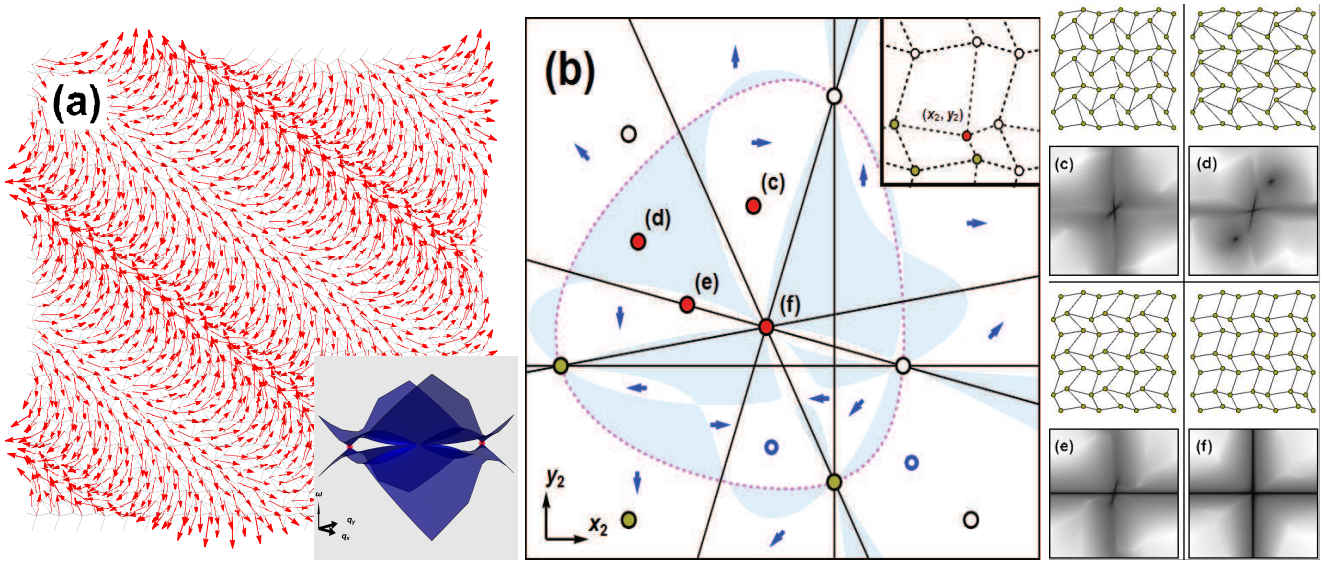

FIG. 1. (a) Deformed square lattices can have sinusoidal bulk zero modes (red arrows) corresponding to Weyl points where two bands touch in the phonon dispersion (inset). (b) The phase diagram of a deformed square lattice with the positions of three sites fixed and the position of the remaining site given by the position (x_2, y_2). The inset shows the three fixed (yellow) sites, one position of the varying (red) site and (white) sites in neighboring crystal cells. (c)-(f) Lattices (top) with phonon dispersions (bottom) with dark areas indicating low-energy modes in the Brillouin Zone. In (b), white areas such as (c) lack Weyl points and are marked with their a blue arrow indicating their topological polarization. Blue-shaded areas such as (d) correspond to Weyl lattices. Open boundaries between white and blue regions indicate where Weyl points emerge at $\boldsymbol{k} = (0, 0)$ while the pink dashed boundary indicate where they annihilate at $\boldsymbol{k} = (\pi, \pi)$. Lattices on the Special Lines, such as (e) lie between topological polarizations and possess lines of zero modes along $k_{x(y)} = 0$, while at the Special Point, (f), there are two zero modes along each of $k_{x(y)} = 0$.

a single basis vector, holding fixed (with dimensionless lengths) lattice vectors $\ell_1 = (1, 0), \ell_2 = (0, 1)$ and basis vectors $\mathbf{b}_1 = (0, 0), \mathbf{b}_3 = (.6, .1), \mathbf{b}_4 = (-.2, .4)$. The resultant 2D phase diagram, shown in Fig. 1(b) exhibits a rich phenomenology: (1) a special point (SP) at the origin with two orthogonal lines of zero modes in its spectrum, (2) special lines (SLs) along which the spectrum exhibits a single line of zero modes, (3) finite regions in which the spectrum is fully gapped and characterized by topological polarizations $\boldsymbol{R}_T$, and (4) finite regions whose spectrum contains Weyl points. Along paths in (4), pairs of oppositely charged Weyl points corresponding to zero frequency *bulk* modes appear at the origin of the BZ along directions with quadratic, rather than linear, dispersions [discussed later in text] and move across the zone edge, annihilating either at the origin or at $\boldsymbol{k} = (\pi, \pi)$. The lattices on the low-dimensional special point and special lines are *critical lattices* that require fine tuning to reach. In contrast, the polarization (3) and Weyl (4) regions occupy extended two-dimensional areas in the phase diagram and do not require special fine-tuning to reach. Because the Weyl modes have zero energy at nonzero wavenumber, lattices in region (4) have an instability that is missed by standard long-wavelength elasticity. The existence of Weyl points has significant consequences for response at the boundaries, leading to a wavenumber-dependent count of boundary modes and SSS.

One can continuously change the crystal basis so as to pass from a lattice of one polarization to another either by crossing a special line *or* by going through a region of Weyl lattices. The latter process, which we now develop in detail, brings pairs of zero modes into and out of the bulk. In contrast, crossing through a critical lattice brings a full line of edge modes into the bulk at a particular point in parameter space.

Lattices of periodically repeated unit cells in d dimensions with n sites (nodes) and n_B bonds per unit cell under periodic boundary conditions (PBCs) are characterized (see Supplementary Material and Refs. [34, 42]) by an $n_B \times dn$ compatibility matrix $\mathbf{C}(\boldsymbol{k})$ for each wavevector $\boldsymbol{k}$ in the BZ relating the dn-dimensional vector $\boldsymbol{u}(\boldsymbol{k})$ of site displacements to the n_B-dimensional vector $\boldsymbol{e}(\boldsymbol{k})$ of bond extensions via $\mathbf{C}(\boldsymbol{k})\boldsymbol{u}(\boldsymbol{k}) = \boldsymbol{e}(\boldsymbol{k})$ and by the $dn \times n_B$ equilibrium matrix $\mathbf{Q}(\boldsymbol{k}) = \mathbf{C}^\dagger(\boldsymbol{k})$ relating forces $\boldsymbol{f}(\boldsymbol{k})$ to bond tensions $\boldsymbol{t}(\boldsymbol{k})$ via $\mathbf{Q}(\boldsymbol{k})\boldsymbol{t}(\boldsymbol{k}) = \boldsymbol{f}(\boldsymbol{k})$. The dynamical matrix (for systems with unit masses and spring constants) is $\mathbf{D} = \mathbf{Q}(\boldsymbol{k})\mathbf{C}(\boldsymbol{k})$. Vectors $\boldsymbol{u}(\boldsymbol{k})$ in the null space of $\mathbf{C}(\boldsymbol{k})$ do not stretch bonds and, therefore, correspond to zero modes. Vectors $\boldsymbol{t}(\boldsymbol{k})$ in the null space of $\mathbf{Q}(\boldsymbol{k})$ describe states with tensions but without net forces and thus correspond to SSSs [43]. The number of zero

modes $n_0(\boldsymbol{k})$ and SSSs $n_s(\boldsymbol{k})$ at each $\boldsymbol{k}$ are related by the generalized Calladine-Maxwell index theorem [34, 43].

$$\nu(\boldsymbol{k}) \equiv n_0(\boldsymbol{k}) - n_s(\boldsymbol{k}) = dn - n_B. \tag{1}$$

In particular, for Maxwell lattices SSSs and zero modes are created only in conjunction with one another, so that the only SSSs in a gapped Maxwell lattice are those associated with the d translational modes. A Weyl point by definition is a $\boldsymbol{k}_w$ at which there is a zero mode, and there is necessarily an SSS that goes with it under PBC. The lines of zero modes occurring along the SLs in the phase diagram also have associated lines of self-stress in real space.

We now turn to zero modes on free surfaces. Cutting a lattice under PBCs along a lattice plane indexed by a reciprocal lattice vector $\boldsymbol{G}$ creates a finite-width strip with two free surfaces aligned along the "parallel" direction perpendicular to $\boldsymbol{G}$. In this case, it is convenient to express $\boldsymbol{k} \equiv (q, p)$ in terms of its components q and p parallel and perpendicular to the cut, respectively. The cut removes Δn_B bonds and Δn sites for each unit cell along its length or equivalently for each wavenumber $-\pi/a_{||} < q < \pi/a_{||}$ along the cut, where $a_{||}$ is the length of the surface cell on the cut. The index theorem relating the total number of zero modes $n_0(q, \boldsymbol{G})$ (counting zero bulk modes at different p) to the total number of SSSs $n_s(q, \boldsymbol{G})$ at each q is

$$n_0(q, \boldsymbol{G}) - n_s(q, \boldsymbol{G}) = \Delta n_B - d\Delta n. \tag{2}$$

Bulk modes in the spectrum are described by the same $\mathbf{C}(\boldsymbol{k})$ as the uncut sample but with a different set of quantized wavenumbers p parallel to $\boldsymbol{G}$. If a bulk mode is gapped in the periodic spectrum, it remains gapped in the strip without an associated state of self-stress. Thus if the bulk modes are gapped at a given q under PBCs, their contribution to the left-hand side of Eq. (2) will be zero, implying that only surface zero modes contribute to Eq. (2). In addition, cutting the sample will not introduce additional SSSs. The result is that Eq. (2) becomes an equation for the total number of zero surface modes on both surfaces, $n_0^{ST}(q, \boldsymbol{G})$. This is a global relation that applies to every q in the surface BZ at which the bulk spectrum is gapped.

As shown in Fig. 2(a), there are multiple ways to define the unit cell, corresponding to different *gauges*. The natural choice in the bulk is a symmetrical cell, but it is possible to obtain the number of zero modes on an edge perpendicular to $\boldsymbol{G}$ directly by selecting a compatibility matrix $\mathbf{C}(\boldsymbol{k}, \boldsymbol{G}) \equiv \mathbf{C}(q, p, \boldsymbol{G})$ in which no bonds cross the edge. As discussed in Ref. [34] and the Supplementary Material, $\mathbf{C}(q, p, \boldsymbol{G})$'s only p-dependent components are proportionate to the complex number $z = e^{i2\pi p/G}$, which is invariant under $p \to p+G$, and not to $z^{-1} = e^{-i2\pi p/G}$. Thus, $\det \mathbf{C}(q, p, \boldsymbol{G})$ has no poles within the unit circle and, by the Cauchy argument principle, its winding number around the circle $|z| = 1$ simply counts the number of its zeros with $|z| < 1$. In contrast, $\det \tilde{\mathbf{C}}(q, p, \boldsymbol{G})$ depends on z^{-1} as well, and it has both poles and zeros within the circle $|z| = 1$, which are counted with opposite signs in the Cauchy integral. A zero of $\det \mathbf{C}(q, p, \boldsymbol{G})$ corresponds to a surface state with a complex inverse penetration depth $\kappa = -\ln z$ with a positive real part indicating decay away from the surface into the bulk. Thus the number of surface zero modes at q is

$$\begin{aligned} n_0^S(q, \boldsymbol{G}) &= \frac{1}{2\pi i} \oint \frac{d \ln \det \mathbf{C}(q, z, \boldsymbol{G})}{dz} \\ &= -\boldsymbol{G} \cdot \boldsymbol{R}_L/(2\pi) + \tilde{n}_0^S(q, \boldsymbol{G}), \end{aligned} \tag{3}$$

where it is understood that $\boldsymbol{G}$ is the *inward* normal to the surface. $\boldsymbol{R}_L = 2\sum_\sigma \Delta \boldsymbol{r}_\sigma - \sum_\beta \Delta \boldsymbol{r}_\beta$, where $\Delta \boldsymbol{r}_\sigma$ is the lattice vector displacement of site σ and $\Delta \boldsymbol{r}_\beta$ displacement of bond β that converts the symmetric cell to the surface cell, is the local polarization introduced in Ref. 16. $\tilde{n}_0^S(q, \boldsymbol{G})$ is the Cauchy integral for the symmetric unit cell. In Weyl-free regions of the phase diagram, $\tilde{n}_0^S$ reduces to the expression, $-\boldsymbol{G} \cdot \boldsymbol{R}_T/2\pi$ derived in Ref. 16.

A Weyl point at $\boldsymbol{k}_w \equiv (q_w, p_w)$ is characterized by an integer winding number

$$n_w = \frac{1}{2\pi i} \oint_C d\mathbf{l} \cdot \nabla_{\boldsymbol{k}} \ln \det \mathbf{C}, \tag{4}$$

where C is a contour enclosing $\boldsymbol{k}_w$. As a result, both $n_0^S(q, \boldsymbol{G})$ and $\tilde{n}_0^S(q, \boldsymbol{G})$ change each time q passes through the projected position of a Weyl point. Consider a lattice with a positive $(+1)$ Weyl point at $\boldsymbol{k}_w^+$ and a negative (-1) Weyl point at $\boldsymbol{k}_w^- = -\boldsymbol{k}_w^+$, and consider a surface with an inner normal $\boldsymbol{G}$ as depicted in Fig. 2(b) for $\boldsymbol{G} = (2\pi/a)(1, 1)$. The number of zero modes at q is calculated from a contour from $p = 0$ to $p = G$ at position q. Choose $q^{1\pm} < q_w^\pm$ and $q^{2\pm} > q_w^\pm$. Because the two paths enclose a Weyl point, the zero-mode numbers on the two sides of the Weyl point differ by the Weyl winding number:

$$n_0^S(q^{2\pm}, \boldsymbol{G}) - n_0^S(q^{1\pm}, \boldsymbol{G}) = n_w = \pm 1. \tag{5}$$

Thus if $n_0^S(q < q_w^+, \boldsymbol{G}) = n_1^S$, the number of zero modes for $q_w^+ < q < q_w^-$ is $n_1^S + 1$, and the number for $q > q_w^-$ is again n_1^S. Figure 3 depicts the real part κ of inverse penetration lengths of surface modes with and without Weyl points. The lengths diverge at the Weyl wavenumbers: the surface mode turns into a bulk mode that traverses the sample.

Domain walls separating two semi-infinite lattices, which we will refer to as the upper and lower lattices as in Fig. 4, with different topological and Weyl characteristics harbor topologically protected zero modes. As in non-Weyl domain walls [16], the index describing the zero mode/SSS count on the wall is governed by the mode counts of the two domains,

$$\nu^D(q, \boldsymbol{G}) = \tilde{n}_{0,L}^S(q, \boldsymbol{G}) + \tilde{n}_{0,U}^S(q, -\boldsymbol{G}), \tag{6}$$

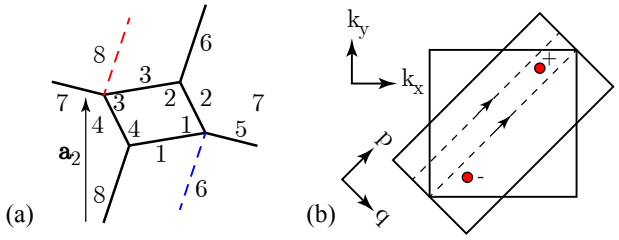

FIG. 2. (a) Different versions of the unit cell with four sites $1-4$ labeled in italic script. The cell consisting of bonds, labeled $1-8$ in roman script and drawn in full black, is the symmetric unit cell. A unit cell associated with a lower (an upper) surface parallel to the x-axis is constructed by moving moving bond 8 through $\boldsymbol{a}_2$ (bond 6 through $-\boldsymbol{a}_2$) to the dashed red (blue) line to yield $\boldsymbol{R}_L = -\boldsymbol{a}_2$ ($\boldsymbol{R}_L = \boldsymbol{a}_2$). (b) depicts the standard square BZ with two Weyl points and the BZ dual to a surface-compatible unit cell oriented at 45°. The component of $\boldsymbol{k}$ along the surface is q and that parallel to $\boldsymbol{G}$ is p. It also shows two paths, one on each side of the projected position q_w^+ the "+" Weyl point at $\boldsymbol{k}_w^+$.

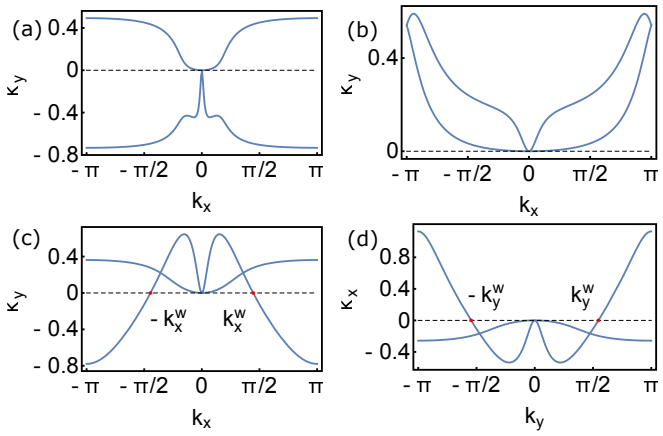

FIG. 3. Real part of inverse penetration depths for fully gapped lattices with no Weyl points [(a) with $\boldsymbol{R}_T = (0,0)$ and (b) with $\boldsymbol{R}_T = (0,1)$] and a lattice (c) and (d) with Weyl points. In (b), a family of zero modes has been shifted from one edge to the opposite relative to the unpolarized case (a), while in (c) and (d) the bulk zero modes are part of families split between two edges.

which now changes across the Weyl wavenumbers [4]. This result, derived and discussed in detail in the Supplementary Material, describes walls with zero modes, self stresses, or *both* (at different wavenumbers).

The long-wavelength elasticity of central-force lattices is determined by the $\boldsymbol{k} = 0$ SSSs [34]. In the lattices we are considering, there are only two $\boldsymbol{k} = 0$ SSSs, implying that there are only two positive definite eigenvalues of the Voigt elastic matrix [44]. There are three independent strains $\boldsymbol{\varepsilon} = (\varepsilon_{xx}, \varepsilon_{yy}, \varepsilon_{xy})$, and the Voigt elastic matrix must have three positive eigenvalues and associated eigenvectors. Thus there must be one macroscopic elastic distortion with strain $\boldsymbol{\varepsilon}^G$ that costs no energy. This is the

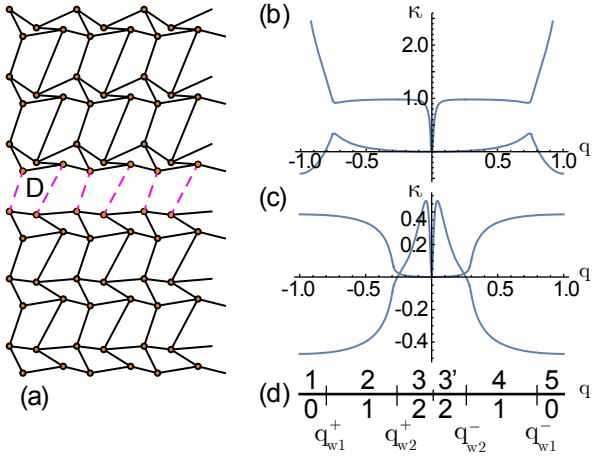

FIG. 4. (a) Two Weyl lattices with differently positioned Weyl points connected at a domain wall D. (b) and (c): the inverse penetration depths of the free surfaces of the upper and lower lattices, respectively. The upper and lower lattices have Weyl points with respective projections onto q of $q_{w1}^{\pm}$ and $q_{w2}^{\pm}$ with $|q_{w2}^+| > |q_{w1}^+|$. The free lower (upper) lattice has two zero modes penetrating downward (upward) for $q_{w1}^+ < q < q_{w1}^-$ ($q_{w2}^+ < q < q_{w2}^-$) and one for $|q| > |q_{w1}^+|$ ($|q| > |q_{w2}^+|$). (d) shows how the two sets of Weyl points divide the surface BZ into five regions with 0, 1, 2, 1, and 0 zero modes in the domain wall. The existence of bulk zero modes at $\boldsymbol{k} = 0$ divides the central region with two zero modes per q into two regions.

Guest mode [45] that is a feature of all periodic Maxwell lattices except those, like the kagome lattice, with extra geometry-driven states of self stress [34]. The long-wavelength determinant of the dynamical matrix equals zero (see Supplementary Material and Ref. [34]) when

$$\frac{k_y}{k_x} = \frac{1}{\varepsilon_{xx}^G}\left[\varepsilon_{xy}^G \pm \sqrt{-\det \boldsymbol{\varepsilon}^G}\right], \tag{7}$$

where $\det \boldsymbol{\varepsilon}^G = \varepsilon_{xx}^G \varepsilon_{yy}^G - (\varepsilon_{xy}^G)^2$ is the determinant of the Guest strain matrix. Thus, to linear order in $\boldsymbol{k}$, there are two lines in the BZ along which there is a zero mode provided $\det(\boldsymbol{\varepsilon}^G) < 0$. Either these modes are raised to finite energy by higher order terms in $\boldsymbol{k}$ not described by the elastic limit, or a single Weyl mode appears along the positive and negative parts of one of the lines. Note that this implies a quadratic rather than a linear dispersion of phonon modes near the origin and leads to inverse decay lengths that are proportional to q^2 rather than q at long wavelengths as shown in Fig. 3.

In this work, we elucidated how Weyl modes generically arise in Maxwell frames and discussed their significance using deformed square lattices as an illustration of the more general phenomenon. Indeed, lattices with larger unit cells have additional phonon bands that more easily touch, generically leading to Weyl points and even multiple pairs thereof [see Supplementary Material]. Thus, our conclusions can be readily extended to other

Maxwell lattices like origami metamaterials [21], random spring networks and jammed sphere packings [46], 3D distorted pyrochlore [47] and stacked kagome lattices [18] that fulfill the Maxwell condition. We also expect the presence of Weyl modes to impact the nonlinear response (e.g. buckling) in the bulk as demonstrated for edge modes [18, 19].

We are grateful to Charles Kane for many informative discussions and suggestions. (DZR) thanks NWO and the Delta Institute of Theoretical Physics for supporting his stay at the Institute Lorentz. MJF was supported by the Department of Defense (DoD) through the National Defense Science & Engineering Graduate Fellowship (NDSEG) Program. This work was supported in part by DMR-1104707 and DMR-1120901 (TCL), as well as FOM and NWO (BGC, VV).

* Current address: Department of Physics, University of Massachusetts, Amherst, MA 01002, USA

[1] N. Nakamura, *Geometry, Topology and Physics*, 2nd ed. (Institute of Physics Publishing, Bristol, 2008) p. 79 and chapter 12.
[2] G. E. Volovik, *The Universe in a Helium Droplet* (Clarenden, Oxford, 2003).
[3] G. Volovik, Lecture Notes in Physics **718**, 3173 (2007).
[4] W. P. Su, J. R. Schrieffer, and A. J. Heeger, Phys. Rev. Lett. **42**, 1698 (1979).
[5] R. Jackiw and C. Rebbi, Phys. Rev. D **13**, 3398 (1976).
[6] B. I. Halperin, Phys. Rev. B **25**, 2185 (1982).
[7] F. D. M. Haldane, Phys. Rev. Lett. **61**, 2015 (1988).
[8] C. L. Kane and E. J. Mele, Phys. Rev. Lett. **95**, 146802 (2005).
[9] B. A. Bernevig, T. L. Hughes, and S.-C. Zhang, Science **314**, 1757 (2006).
[10] J. E. Moore and L. Balents, Phys. Rev. B **75**, 121306 (2007).
[11] L. Fu, C. L. Kane, and E. J. Mele, Phys. Rev. Lett. **98**, 106803 (2007).
[12] Z. Hasan and C. Kane, Rev. Mod. Phys. **82**, 3045 (2010).
[13] X.-L. Qi and S.-C. Zhang, Rev. Mod. Phys. **83**, 1057 (2011).
[14] E. Prodan and C. Prodan, Phys. Rev. Lett. **103**, 248101 (2009).
[15] M. J. Lawler, New J. of Phys. **15** (2013).
[16] C. Kane and T. C. Lubensky, Nature Phys. **10**, 39 (2014).
[17] J. Paulose, B. G. Chen, and V. Vitelli, Nature Physics **11**, 153 (2015).
[18] J. Paulose, A. S. Meeussen, and V. Vitelli, Proceedings of the National Academy of Sciences of the United States of America **112**, 7639 (2015).
[19] B. G. Chen, N. Upadhyaya, and V. Vitelli, Proceedings of the National Academy of Sciences of the United States of America **111**, 13004 (2014).
[20] V. Vitelli, N. Upadhyaya, and B. G. Chen, arXiv:1407.2890 (2014).
[21] B. G. Chen, B. Liu, A. A. Evans, J. Paulose, I. Cohen, V. Vitelli, and C. D. Santangelo, Arxiv (2015).
[22] M. Xiao, G. Ma, Z. Yang, P. Sheng, Z. Q. Zhang, and C. T. Chan, Nature Physics **11** (2015), 10.1038/nphys3228.
[23] H. C. Po, Y. Bahri, and A. Vishwanath, (2014), arXiv:1410.1320.
[24] Z. Yang, F. Gao, X. Shi, X. Lin, Z. Gao, Y. Chong, and B. Zhang, Physical Review Letters **114**, 114301 (2015).
[25] L. M. Nash, D. Kleckner, V. Vitelli, A. M. Turner, and W. T. M. Irvine, Arxiv (2015), arXiv:1504.03362v1.
[26] P. Wang, L. Lu, and K. Bertoldi, Arxiv (2015), arXiv:1504.01374v1.
[27] Y.-T. Wang, P.-G. Luan, and S. Zhang, New Journal of Physics **17**, 073031 (2015).
[28] R. Susstrunk and S. D. Huber, Science **349**, 47 (2015), 1503.06808v1.
[29] T. Kariyado and Y. Hatsugai, arXiv:1505.06679 (2015).
[30] V. Peano, C. Brendel, M. Schmidt, and F. Marquardt, Phys. Rev. X **5**, 031011 (2015).
[31] S. H. Mousavi, A. B. Khanikaev, and Z. Wang, arXiv:1507.03002 (2015).
[32] A. B. Khanikaev, R. Fleury, S. H. Mousavi, and A. Al, Nat. Comm. **6** (2015).
[33] D. Z. Rocklin, S. Zhou, K. Sun, and X. Mao, arXiv:1510.06389 (2015).
[34] T. C. Lubensky, C. L. Kane, X. Mao, A. Souslov, and K. Sun, Reports on progress in physics. Physical Society (Great Britain) **78**, 073901 (2015).
[35] X. G. Wan, A. M. Turner, A. Vishwanath, and S. Y. Savrasov, Physical Review B **83**, 205101 (2011).
[36] A. A. Burkov and L. Balents, Physical Review Letters **107**, 127205 (2011).
[37] A. A. Burkov, M. D. Hook, and L. Balents, Physical Review B **84**, 235126 (2011), burkov, A. A. Hook, M. D. Balents, Leon.
[38] J. P. Liu and D. Vanderbilt, Physical Review B **90**, 155316 (2014).
[39] S.-Y. Xu, I. Belopolski, A. Nasser, M. Neupane, G. Bian, C. Zhang, R. Sankar, G. Chang, Z. Yuan, C.-C. Lee, S.-M. Huang, H. Zheng, J. Ma, D. S. Sanchez, B. Wang, A. Bansil, F. Chou, P. P. Shibayev, H. Lin, S. Jia, and M. Z. Hasan, Science **249**, 613 (2015).
[40] L. Lu, L. Fu, J. D. Joannopoulos, and M. Soljacic, Nature Photonics **7**, 294 (2013).
[41] L. Lu, Z. Wang, D. Ye, L. Rain, J. D. Joannopoulos, and M. Soljacic, Arxiv:1502.03438v1 (2015).
[42] K. Sun, A. Souslov, X. Mao, and T. C. Lubensky, PNAS **109**, 12369 (2012).
[43] C. R. Calladine, Int. J. Solids Struct. **14**, 161 (1978).
[44] N. W. Ashcroft and N. D. Mermin, *Solid State Physics*, 1st ed. (Cenage Learning, New York, 1976).
[45] S. D. Guest and J. W. Hutchinson, J. Mech. Phys. Solids **51**, 383 (2003).
[46] D. M. Sussman, O. Stenull, and T. C. Lubensky, unpublished (2015).
[47] O. Stenull, C. L. Kane, and T. C. Lubensky, unpublished (2015).